Observation and simulation of indentation damage in a SiC-SiC_{fibre} ceramic matrix composite[1]

Luis Saucedo-Mora[*a], Mahmoud Mostafavi [b], Danial Khoshkhou [c], Christina Reinhard [d], Robert Atwood [d], Shuang Zhao [e], Brian Connolly [c] and T. James Marrow [a]

[a] University of Oxford Department of Materials, Parks Road, Oxford OX1 3PH, United Kingdom
University of Sheffield, Department of Mechanical Engineering
Sir Mappin Building, Mappin Street, Sheffield S1 3JD, United Kingdom
[c] University of Birmingham, Department of Metallurgy and Materials, Birmingham, B15 2TT, United Kingdom
[d] Diamond Light Source, Harwell Science and Innovation Campus, United Kingdom
[e] Key Laboratory of Advanced Ceramic Fibers and Composites, National University of Defence Technology, Changsha, China
[*]e-mail: luis.saucedomora@materials.ox.ac.uk

[1] This is the author's pre-review copy of a paper subsequently published in Finite Elements in Analysis and Design 110 (2016) 11–19, http://dx.doi.org/10.1016/j.finel.2015.11.003

Abstract

FEMME, a multi-scale Finite Element Microstructure MEshfree fracture model has been applied to simulate the effect of microstructure on the development of discontinuous cracking and damage coalescence during the Hertzian indentation of a SiC-SiC fibre composite. This was studied experimentally by digital volume correlation analysis of high-resolution synchrotron X-ray computed tomographs, which quantified the damage via measurement of the 3D displacement fields within the material. The experimental data are compared with the model simulations, and demonstrate the applicability of the modelling strategy to simulate damage development in a heterogeneous quasi-brittle material.

Keywords: X-ray computed tomography, Digital Volume Correlation, Hertzian indentation, microstructure, SiC-SiC fibre composite, Finite Elements, Meshfree, Multi-scale.

Introduction

SiC-SiC$_{fibre}$ ceramic matrix composites are candidate materials for high temperature fuel cladding in Generation IV gas-cooled nuclear reactor concepts; they have also been proposed for accident-tolerant fuel cladding for current (Gen II/III) light water reactors and have potential applications in the breeder blanket of nuclear fusion power [1, 2, 3, 4]. The influence of microstructure on fracture resistance in these materials is significant, and for this reason microstructure needs to be introduced into predictive modelling of structural integrity. In the context of nuclear fission applications, a particular goal is to predict the influence of microstructure on fuel-cladding integrity and the effects of its degradation, both under normal service and extreme conditions, in order to select materials and to optimise the methods for fabrication and testing of fuel clad. It is critical that predictive models that support design and safety assessments are founded on data, which must be obtained in representative conditions. Ultimately, there will be a need to obtain data from irradiated materials, tested in realistic conditions (i.e. >1000°C). However, due to the necessity of examining multiple conditions within time-constrained material test reactor (MTR) accelerated-ageing irradiation programmes, such studies inevitably require small test specimens for which the length scale of the composite microstructure is significant compared to the sample size; this can introduce heterogeneity and scatter into the data due to the local behaviour of microstructure. To interpret such tests, it is necessary to have modelling techniques that are sensitive to both the microstructure and the specimen geometry and size.

Indentation is a common test method to measure material properties in small specimens, and also to investigate the local behaviour of features in microstructures; for instance, microindentation [5,6] has been used to obtain interfacial properties in fibre-reinforced composites. But indentation testing is a surface characterisation technique, and except in transparent materials or via destructive analysis, the assumed damage and deformation processes are not directly observed. Greater understanding of indentation testing may be obtained, and utilised to validate models that simulate local microstructure effects, if the deformation within the material is observed. This can be done in appropriate microstructures using X-ray computed tomography (XCT) in combination with three-dimensional digital image correlation (digital volume correlation or DVC) [7,8] to measure the displacements within materials [9,10,11]; sufficient contrast may be achieved by X-ray attenuation or scattering from microstructural heterogeneities of the order of the voxel[2] size. The precision of displacement resolution increases with the multi-voxel interrogation subset size, enabling DVC to measure sub-voxel displacements [12]; recently this method has been used to characterise, for instance, the fracture behaviour of polygranular quasi-brittle materials [13,8], indentation cracking in brittle polycrystalline ceramics [14] and the plastic zones beneath hardness indentations in engineering alloys [15].

SiC-SiC$_{fibre}$ ceramic composite is an example of a quasi-brittle material. Such materials have heterogeneous structures, typically with brittle constituents, and this important class of structural materials includes concrete, polygranular nuclear graphite, zirconia toughened alumina, geological structures and also biomedical materials such as bone and bone replacements. Their damage or defect tolerance is much less than metallic engineering

[2] A voxel is the three-dimensional equivalent to a pixel

alloys, but can be quite significant compared to monolithic ceramics. Quasi-brittle fracture is an emergent characteristic that cannot be treated satisfactorily with numerical methods based on macromechanics. As a consequence of their complex microstructure, the continuum approach needs very fine discretization to obtain satisfactory results [e.g. 16,17,18,19]. In numerical terms, this means that the computational cost of advanced methods, such as cohesive elements or embedded cracks, can be too high for engineering scale problems. However, including the microstructure is necessary to reproduce structural behaviour in these materials. To address this, various multiscale modelling approaches such as Homogenization, Monte Carlo, Cellular Automata and Molecular dynamics [e.g. 20,21,22] have been proposed as methods to reproduce microstructure within a larger continuous element or Representative Volume Element (RVE); this introduces microstructure into a continuous FEM model. Nonetheless, there remain challenges due to high computational cost and mathematical complexity that hinder the application of these methods for different loading conditions in complex geometries, or more detailed 3D representation of the microstructure.

In this paper we apply the novel FEMME model [22, 35, 36] in a case study for microstructure-sensitive damage development in a quasi-brittle material: Hertzian indentation in a SiC-SiC_{fibre} composite. FEMME is a multi-scale Finite Element Microstructure MEshfree fracture model for materials with complex microstructures. The combined techniques of computed X-ray tomography and digital volume correlation have been used to characterize the microstructure and its response to indentation damage in order to test the FEMME modeling approach. The paper is structured as follows: first we describe the mechanical properties and fabrication process of the SiC-SiC composite; after this, the experimental program and the analysis of the data are explained. From those results we describe the application of the FEMME numerical model to simulate the interaction between the microstructure and the Hertzian indentation, validating this against the experimental results.

Material

The SiC/SiC_{fibre} composite was produced in three steps: (i) preparation of the SiC fibre performs; (ii) deposition of the fibre coating; and (iii) final fabrication of the SiC/SiC composites. The 3-dimensional 4-directional (3D4d) fibre preforms were woven by Bolong Co. Ltd (China), with a fibre fraction volume of approximately 40 %. The KD-I SiC fibre used, made by the National University of Defence Technology, China [23] has a diameter of 12.5 μm, tensile strength of 1.6-2.0 GPa and a density of 2.4 g/cm^{-3}. This is a polymer-derived multiphase fibre consisting of β-SiC crystalline, Si-C-O amorphous and free carbon phases. A pyrolytic carbon (PyC) coating was deposited onto the surface of the fibres to form the fibre/matrix interphase through a CVD (Chemical Vapor Deposition) process. The composite was fabricated via the PIP (Polymer Infiltration and Pyrolysis) process; the polycarbosilane precursor (PCS) was infiltrated into the preform and heated up to 1100°C in an inert atmosphere, with the infiltration and pyrolysis process repeated for about 10 cycles until weight increase was less than 1%. The final heat treatment was at 1400°C for 1 hour in an inert atmosphere.

Three-dimensional Experimental Characterisation of Microstructure and Indentation Damage

The three-dimensional microstructure of the sample was characterised by X-ray computed tomography, with the development of damage from indentation measured using

digital volume correlation of the tomography images. The tomography was performed at the UK Diamond Light Source, Joint Engineering, Environmental and Processing beam line (I12 – JEEP), using radiographic projections obtained at an X-ray beam energy of 53 keV with a nominal voxel size of 0.9 μm. The exposure time was 2 seconds per radiograph with projections at increments of 0.03 degrees over 180° rotation. The specimen, is a cube of 3×3x3 mm cut using a diamond saw from a larger sample, was indented by a 5 mm radius ZrO_2 ball under displacement control using a loading stage that had been modified to accommodate the indenter. The indentation was applied to an as-received surface.

A reference tomograph was recorded before indentation under a small pre-load (10 N), applied to reduce rigid body movement between successive scans, then a scan was recorded in situ under a maximum applied load of 275 N (the final indentation depth was 43 μm, measured from radiographs under load); this dropped to 245 N during the tomography scan. A combined Fourier-wavelet ring artefact removal algorithm [24] was used to suppress ring artefacts in the reconstructed tomographs.

Vertical slices through the tomography data are shown in Figure 1 at the position of the indenter, before and during indentation. The complexity of the microstructure is clear; large macro-pores, fine micro-pores and oriented bundles of fibres with elongated inter-fibre pores are observed. The damage induced by the indentation occurs over a length scale (~0.5 mm) that is comparable to the length scale of the microstructure (circled in Figure 1).

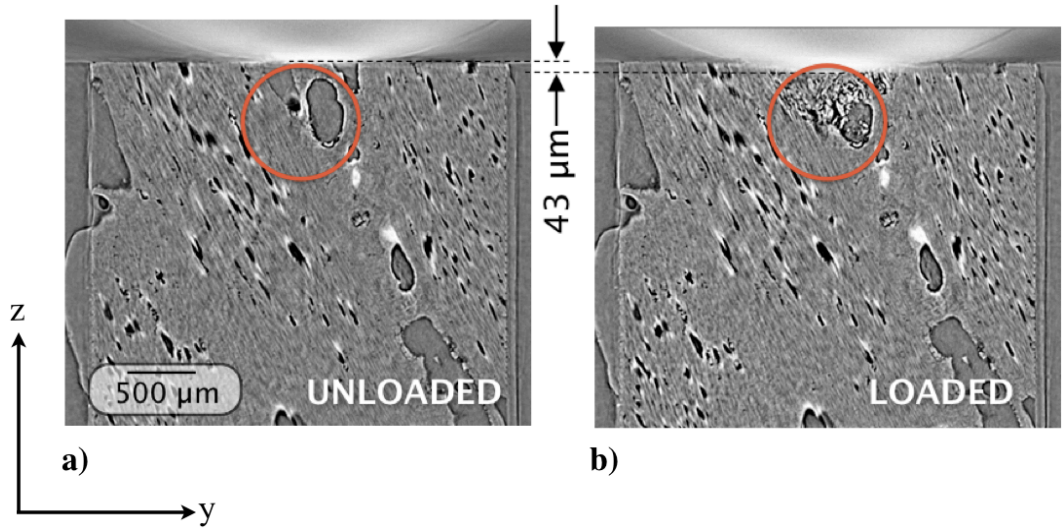

Figure 1: Vertical slice through the tomographic image of the SiC-SiC$_{fibre}$ sample at the position of the indenter; a) before indentation, b) in situ under indentation. The visible damage zone is enclosed within a red circle, and this is also marked in subsequent figures.

The tomographic data were analysed using the Avizo Fire software (Version 7.0) to obtain a statistical description of the porosity. To reduce noise, 3-D median image filtering was applied to prepare the data sets before segmentation, which was done by contrast thresholding. Groups of inter-fibre pores were identified, each group was assigned a unique label field material, with fifteen groups observed in the analysis volume. The 3-D material statistics collected for each inter-fibre pore including 3-D volume, length, width, orientation and the spatial coordinates of the pore's origin. Binary thresholding was performed to define a bounding volume for each group of inter-fibre pores, with centreline

trees evaluated for each pore group to obtain the mean radius and tree length. A similar analysis was also carried out to obtain the statistics of the small micropores (i.e. < 15 μm) and larger macropores (i.e. >125 μm) in the matrix.

The DVC analysis was carried out using the Davis StrainMaster 8.1 software [25], correlating the loaded 3D tomographic dataset against the unloaded reference. Each dataset was cropped to 3500×3500×2000 voxels and converted to 8 bit data for the analysis. The coarse vertical (z) rigid body movement (~ 50 μm) between datasets was corrected prior to image correlation by visual matching of image slices in a horizontal xy plane close to the indented surface; coarse translations of 32 μm in x and 49 μm in y were similarly applied. These displacements arise from the compliance of the loading jig. The following image correlation parameters were judged to be optimal in terms of precision and grid density of the displacement field matrix; 256×256×256 voxel interrogation window (a.k.a. interrogation subset), 50% overlap and 1 pass, followed by 64×64×64 interrogation window, 50% overlap and 2 passes. Reducing the final interrogation window size in image correlation increases the displacement map spatial resolution, though excessive noise arises with smaller window size [26]. Overlapping interrogation windows improve the displacement map spatial resolution in smoothly changing fields, allowing the use of larger interrogation windows to reduce measurement noise. Increasing the number of passes may also reduce noise, with a diminishing effect with increasing passes. Finally, the remaining minor (i.e. sub-voxel) rigid body translations and rotations were corrected [15] such that the relative displacements remote from the indentation, i.e. close to the bottom surface of the sample, were zero.

Example tomographic virtual slices, with the corresponding displacement fields, are shown in Figure 2 for a vertical (z-y) section through the centre of the indentation and also for a horizontal (x-y) section approximately 217 μm below the indentation. There is a zone of poor correlation immediately below the indentation, which is due to the effects of damage; significant changes in the image will prevent DVC from converging. Comparison of the images indicates that the asymmetry of the displacement field is caused by the fibre orientations in the microstructure; larger displacements are observed where the imposed deformation is perpendicular to the fibre axis, which is to be expected to due to the anisotropy of elastic moduli. Greater displacements also tend to be associated with the larger macropores, indicating that these have a local effect on deformation. These data demonstrate that the DVC analysis of the tomography data is sensitive to the effects of the microstructure.

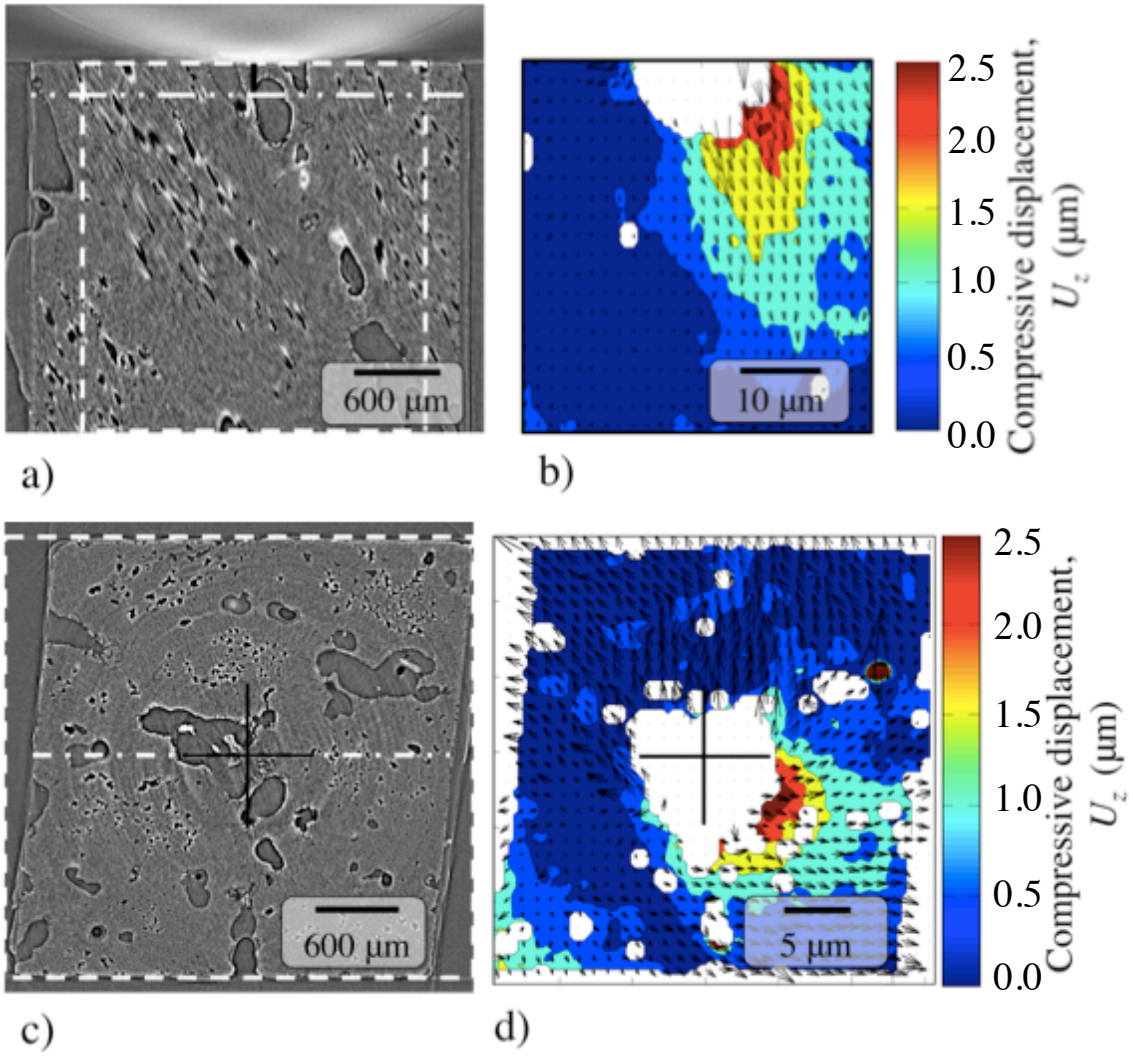

Figure 2: Sections of the tomography data (prior to indentation) and the corresponding displacement fields due to the indentation. The white areas have poor correlation coefficient (C<0.5) and have been censored. The data are shown for a vertical (z-y) section through the indentation centre in a) and b) and for a horizontal (x-y) section beneath the indentation in c) and d). The white dashed box in each tomograph section outlines the region within which the corresponding displacement data are represented, and the position of the indentation is marked with a cross in the horizontal sections. The white dash-dot line in the tomographs represents the intersection of the vertical and horizontal sections. The scale bar in the tomograph sections shows the length scale of the images, whereas that in the displacement fields (which are shown at the same magnification) represents the length scale of the displacement vectors. The displacement data are presented using contours for the vertical (z) compressive displacement, with vectors showing the direction and magnitude of the in-plane displacements within the section. For clarity, only 1/9 of the full data are presented in each section.

Numerical Modelling of Damage using the FEMME (Finite Element microstructural adaptive MEshfree) model

We have used a novel FEMME method, which employs Cellular Automata (CA) integrated with Finite Elements (FE) and a Microstructural Adaptive Meshfree (MAM) framework). This method is described in detail in reference [22, 35, 36], and a brief summary is provided here only. The Meshfree framework has been developed to simulate

fracture development, using the CA to calculate the damage in the microstructure. In this method the microstructure is modelled explicitly, when required, by subdividing a finite element into smaller elements called cells. The heterogeneous microstructure is created from key cells, called seeds, from which particle-like regions may be grown with defined characteristics. By this topological approach we obtain sets of cells with variable properties to model the microstructure (rules are enforced during the selection of the seeds to avoid overlap between particles). The influence of the initial FE mesh is erased during the development of the microstructure. The development of discontinuous cracking and fracture, and its sensitivity to microstructure, is simulated using two layers of elements representing the finite element model and the microstructure. The first is used to link the engineering scale problem with the microstructure, obtaining the stress and strain fields of the macromechanical problem.

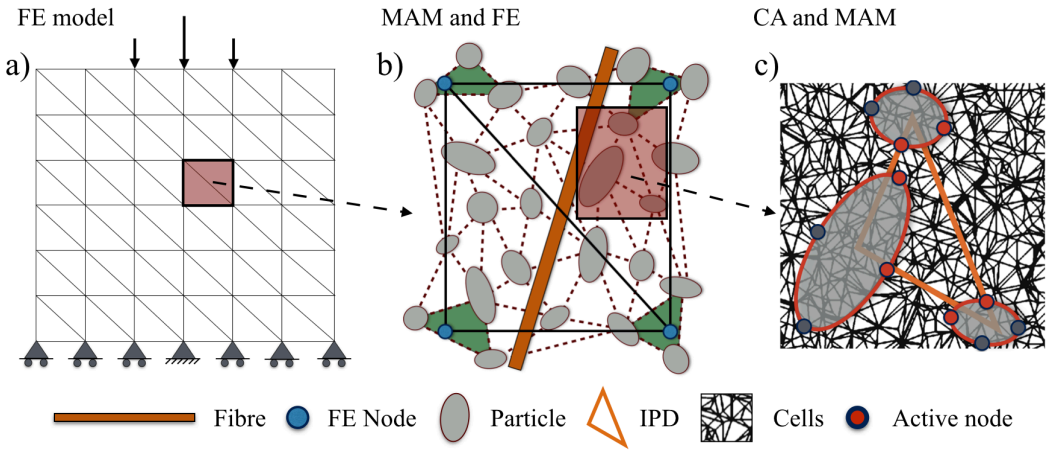

Figure 3: 2D scheme of all the layers of the model; the Finite Element Model (FEM) that reproduce the macromechanical model, the Microstructural Adaptive Meshfree model (MAM) that calculates the displacements in the microstructure and the Cellular Automata model (CA) that carries all the fracture information of the different phases.

All the layers in the model are linked and share information; the nodal displacements of one layer are the input to the next layer. Thus, from the displacements of the FE model the boundary conditions of the Meshfree model are created. These are inserted by fixing the displacement of a particle or IPD (Inter Particle Domain, which is the domain between particles that represents the matrix - a pore is an 'empty' particle) according to the displacement of the hosted FE node. This is the case shown in Figure 3b where the displacements of the blue nodes are imposed in the green IPDs. The damage is completely free with respect to the FE mesh, and consequently, very complex fracture behaviour can be modelled, such as multiple or discontinuous cracks. Once the displacements of the microstructural features are calculated with the MAM layer by solving equation 1, the displacements are mapped to the cells of the CA model. This is done with the exponential shape functions of the IPD or PD that interpolate the domain [22]. With the displacements of the cells, the strains are computed and evaluated against the critical strain of the material phase that it represents.

$$[K]_{MAM} \cdot \bar{b} = \overline{\delta} \qquad (1)$$

Equation 1 shows the mechanical model that is solved in the MAM layer. The calculation of the matrix K is explained in detail within references [22] and [35]. The boundary conditions are applied by fixing the displacement of the IPDs or PDs that host a FE node inside, to ensure the deformation given by the FEM in the microstructure. The

vector b is used in other applications of the model, such as [36], to insert the internal forces in the microstructure produced by thermal expansion.

In the present model, the fibres are not inserted explicitly in the mechanical framework that calculates the displacements of the microstructural features (MAM), but this is planned for future applications. Here, they are inserted implicitly by assigning different mechanical properties to the cells that represent the fibres, as also to the cells that represent the longitudinal or elliptical pores. Using a local "rule of mixtures", the mechanical properties of the Meshfree domains (i.e. IPD and PD) are varied according to the proportion of cells within them that belong to the different phases.

We have introduced a variation with respect to the initial FEMME model [22, 35, 36] in this work to improve the computational cost in the solution of this composite sample. In the full model, there is two-way communication between the Meshfree and CA layers as well as between the FE and Meshfree layers. In this application, we have replaced the inverse relationship of homogenization between the Meshfree and FE layers by a cohesive law (Figure 4). This increases the efficiency in reaching an equivalent solution as the overestimate of the total energy of the system, which arises from the coarse FE mesh, is addressed by adjustment of the arbitrary limits of the cohesive law. In this way the damage model is developed in isolation within the FE layer, and the final displacements of this layer are the boundary conditions of the Meshfree method, which are imposed as described in [22]. This assumption is reasonable since the aim of the model is to reproduce the global state of the material in order to improve the understanding of its internal processes. Hence the global response of the composite is used to calibrate the local behaviour of the microstructural features. The method is explained in some detail within the description of the simulation of Hertzian indentation, further in this paper.

It is necessary to have a damage model as a material property to do this, and here the cohesive law is estimated from the known mechanical properties of the composite and its constituents, summarised in table 1. As a first approximation a simple 4-parameter damage model was used (Figure 3). The critical strain at which damage develops in either tension (ε_{ct}) or compression (ε_{cc}) is given by the ratio of relevant strength and Young's modulus [27,28]. From the known composite flexural strength of ε_{ct} = 0.003 [5]. The maximum or final tensile strain (ε_{ft}) is arbitrarily three times the critical tensile strain. The compressive critical and final strains were obtained by fitting the numerical reaction force of the indentation simulation to the experimental measurement, hence the obtained values are ε_{cc} = 0.01 and ε_{fc} = 0.24 respectively, with an associated critical compressive strength of 626 MPa; this is consistent with the reported range of 650-750 MPa of such composites [28].

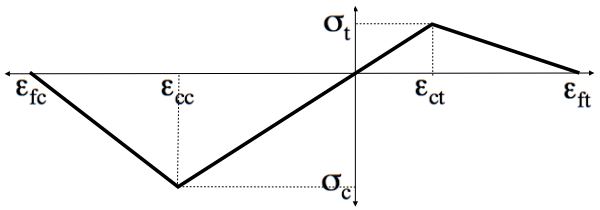

Figure 4: The 4-parameter cohesive damage model used in the FEM simulations of the SiC-SiC$_{fibre}$ composite

Table 1: Mechanical properties of the SiC/SiC$_{fibre}$ composite, measured by nano-indentation for the fibres and the matrix and in flexure for the composite [5]

E (GPa)	E (GPa)	E (GPa)	σ_t (MPa)
Fibre	Matrix	Composite	
115	188	85.4	257

A key advantage of this method is the capability to reproduce the microstructure and simulate its damage, and thereby to insert discontinuities into the continuum model. To test its application to damage development, it is necessary reproduce numerically the significant microstructure features that are observed experimentally; these are the inter-fibre pores that create paths of weakness, and also the significant macro pores that are stress concentrators. Rather than directly copy the observed features, the elongated inter-fibre pores were distributed in the simulation of the specimen within the identified bounds of the 15 groups of fibre bundles, with their dimensions, orientation and position defined randomly using parameters from their measured statistical distributions (Figures 5 and 6). A total of 30 macro pores, with ellipsoidal shape and with radii from 0.125 mm to 0.295 mm, were similarly distributed randomly in the matrix (Figures 6 and 7). The simulation therefore consisted of SiC matrix and SiC fibres within the 15 fibre bundles with mechanical properties given in Table 1, and empty pores. The experimentally observed pores around the fibres are inserted touching the fibre surface (Figures 6 and 7), with a radius of 0.005 mm. The average cell size is 0.03 mm, so those pores are represented by the individual cells which has its centre closer than 0.005 mm from the fibre surface. Finally, to increase the discretization in the Meshfree layer, 800 spherical micropores with a diameter equal to the cell size (0.015 mm) are inserted randomly in the domain. These have no mechanical effect. Together, these represent the total observed porosity of 19%, with 99% of the porosity represented by the macro-pores.

Different material properties are assigned to each phase via the subdivision of the FE into cells and the evaluation of the cell position against the geometrical representation of every phase; each cell is either within or outside a pore (3D ellipsoids of varying orientation and size) or a fibre (cylinders with different orientations and variable thickness). A number of simulations were developed; for consistency with the actual experiment a simulation was selected that had a large pore close to the indentation point (Figures 7, 8 and 9).

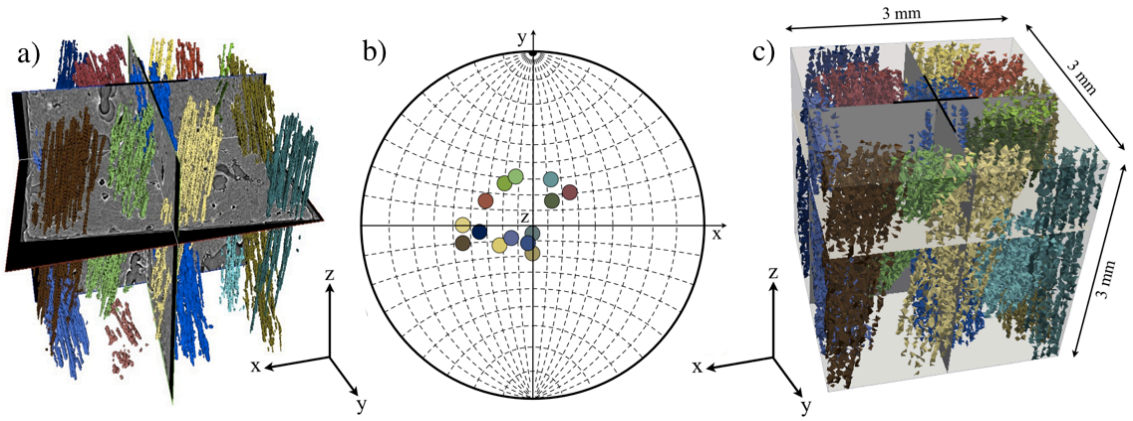

Figure 5: Inter-fibre pore distributions within fibre groups: a) experimentally observed structure after segmentation; b) stereographic projection pole figure of the fibre tow orientations; c) numerical simulation. Each colour identifies a single fibre tow.

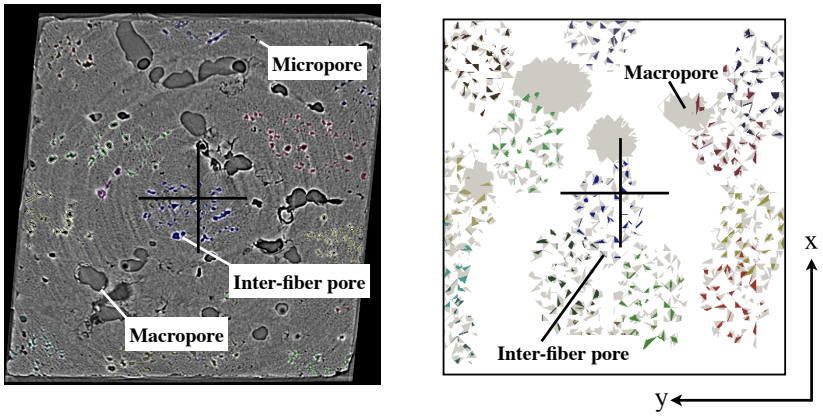

Figure 6: A 2-dimensional section of the macro and micropore distributions in the matrix: a) experimentally observed structure after segmentation; b) numerical simulation

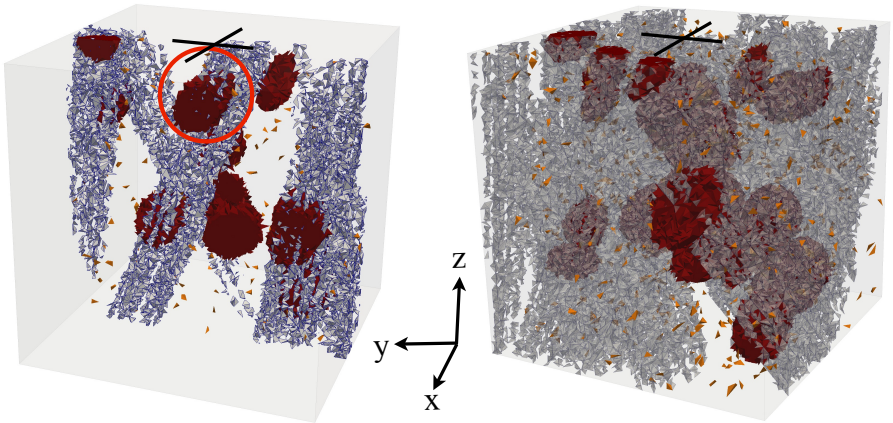

Figure 7: Overall view of the structure in the numerical simulation: fibres (white), macro-pores (red) and micro-pores (orange) a) cross-section, b) surface view. The cross shows the indentation point, and the red circle the macro-pore beneath the indenter, which reproduces a real macro-pore.

Simulation of Hertzian Indentation

The Hertzian indentation was simulated without an explicit representation of the ball by inserting the displacement of the indenter contact surface directly as the boundary condition in the FE model. Since a coarse FE mesh is used in the FEMME model, the inserted boundary conditions need to be verified against analytical functions to ensure that the real loading conditions are reproduced. This established approach [29,30,31] is governed by the theory of Hertz; equation 1 provides the contact area (i.e. a circle with radius α). Similarly, the reaction force, P produced by the indenter for an elastic material with displacement δ applied to the ball is given by equation 2:

$$\alpha = \sqrt{\delta R} \tag{2}$$

$$P = \frac{4}{3}\alpha E^{*}\delta \tag{3}$$

From the experimental observations, δ=0.043 mm is the vertical displacement of the indenter into the material, giving a contact area radius α=0.46 mm through equation 1. The homogenized Young modulus, E*=85.4 GPa, assumes Poisson's ratio of 0.2. The vertical displacements imposed on the nodes affected by the contact are equal to the penetration of the ball at that point. This approximation is valid for small contact radius (i.e. $\alpha<0.2R$); friction is not considered [32]. Due to the nodal distances of the coarse FE mesh, the boundary conditions could only be imposed over a minimum radius of 0.5 mm, rather than the actual contact radius of 0.46 mm. A homogeneous elastic FE simulation with the same boundary conditions and mesh obtained a reaction force, P, of 2.34 kN (c.f. 2.27 kN via equation 2, and 2.75 kN as the experimental measurement). This validates the boundary conditions applied; the resultant force from a FE model being typically slightly higher than the theoretical counterpart [33]. The close agreement obtained experimentally and through equation 2 also shows that this assumption is reasonable.

The FEMME simulation aims to describe the heterogeneous development of damage at the microstructure scale, whilst being consistent with the deformation at the continuum macroscale. The continuum scale is addressed first; the initial isotropic Young's modulus of each element is the homogenization of the microstructure within, using a local "rule of mixtures" from the known pore and fibre volumes within each element. As damage creates further pores or cracks, the Young's modulus of each element changes; so to simulate the continuum effects of damage, the material properties of the finite elements are recomputed according to the imposed damage criterion described by the cohesive law of Figure 3. This is done by iteration, reducing the Young's modulus of the elements to relax the stresses of the FE layer and accommodate the displacement of the indenter until the critical tensile or compressive strength of the material is no longer exceeded. This method is an alternative to the Hill-Mandell energy homogenization theorem applied previously in FEMME [22,35,36]. It is done to reduce computational costs in this particular problem, which has a high level of discretisation due to the representation of the fibres in the whole volume; by using a cohesive law to replace the cohesive behaviour that emerges from the energy homogenization [22] the iterations only need to be carried out in the FE layer. The model only has one load step to simulate, and the damage is distributed in a local region. The factor by which the modulus of damaged elements was reduced is given by the energy release through the defined cohesive law. Once this is achieved, the nodal displacements of the relaxed FE layer are used as an input of the Meshfree framework that deals with actual damage in the microstructure layer. A similar iterative relaxation is carried out in the microstructure layer to fit the nodal displacements of the FE layer, introducing damage into cells in which the critical strain is exceeded [22,35,36]. At every

step, cells were identified with a strain coefficient above unity, (i.e. strain/critical strain); these were treated as damaged and were therefore eroded.

Consequently, the pattern of damage produced in the microstructure is consistent with the imposed boundary conditions and the heterogeneity of material properties. The global model provides the same response (i.e. the same reaction force) to the same boundary conditions (i.e. displacement of the indenter) as the experimental counterpart. Different simulations were run to investigate the effects of the inter-fibre pores; first with both the inter-fibre pores and macro-pores, secondly with just inter-fibre pores, thirdly just the macropores (all simulations contain micro-pores in the matrix). The full FEMME simulation contained 830 pores (1105950 cells and 4980 nodes, i.e. 6 nodes per pore), the inter-fibre pores are not considered in the Meshfree model but are treated as eroded cells in the CA layer in order to reproduce their strain intensification effect; the simulation's computational cost was 7.5 hours running as a serial code as a single thread, where 550 seconds were used for the homogeneous continuum FE simulation of the first layer (343 nodes and 1080 tetrahedral elements), all running on a Intel Core i7-3930K, 3.20 GHz machine.

Comparison between Experimental Observation and FEMME Simulation

The sensitivity of the FEMME simulation to the microstructure components is illustrated in Figure 8. This shows the results for different simulations: (i) with both the inter-fibre pores and macro-pores; (ii) with just interfibre pores; and (iii) also just macropores, compared with the continuum FE layer. In the FEMME simulations, the dark gray colour denotes damaged cells in which the critical strain was reached. This shows that close to the indentation most of the fibre boundaries, which are the weakest part of the microstructure, have failed. Because the failure is mainly produced in the inter-fibre zones, the damage in the matrix is not shown but it is implicit in the reduction of the modulus in the FE layer. This splitting failure mode [28] (i.e. tensile cracking along the fibre direction) is the typical failure modes in fibre ceramic composites under a compressive concentrated load [34]. The extent of the damage (~1 mm) is consistent with the experimental observation (Figure 1). Comparing the simulations with and without macro-pores (Figure 8a and b), it can be seen that there is increased deformation and damage where a macro-pore is close to a bundle of inter-fibre pores. This is due to the stress concentrating effect of the macro-pores, which is also seen in the absence of fibres (Figure 8c), where larger displacements are observed in the vicinity of the macro-pores. Figure 8d shows the continuum damaged FE model.

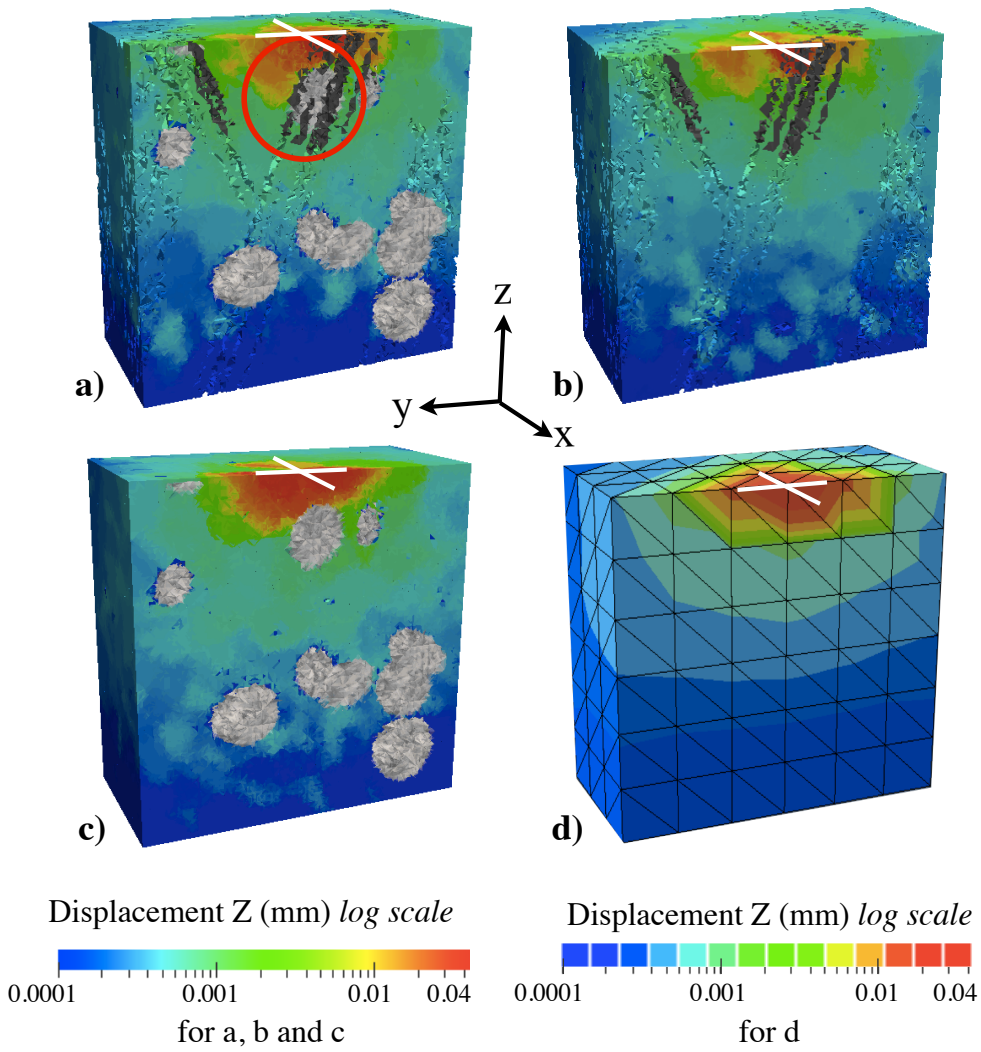

Figure 8: Influence of the pores and fibres on the compressive displacement field; FEMME simulation with a) macro-pores and inter-fibres pores, b) inter-fibre pores only, c) macro-pores only, and d) FEM simulation with damage

A more quantitative comparison is obtained by considering the compressive displacements and strains along the vertical *z*-axis through the indentation centre (i.e. at *x*=1.5 mm and *y*=1.5 mm). These are shown for the FEMME simulation in Figure 9; quarter sections of the numerical simulation are presented in which the macro-pores are shown together with the FE layer that describes the continuum. As the simulation cells are not necessarily located exactly on the *z*-axis, the displacement data for all of the cells within 1/30 of the side length (i.e. 100 μm) from the *z*-axis are shown; the average strain values from those cells located on the z-axis are shown. A comparison is also made with the displacements and strains from an elastic FE simulation (i.e. with constant modulus) for the same reaction force.

The agreement between the experiment and the simulations with damage is generally good, particularly remote from the indentation where the deformation is elastic. Such general agreement between the FEMME simulation and FE layer is to be expected, as they are linked. The interest is in the variability of the FEMME displacements, which arises from

the local effects of pores on the development of damage. For instance, there is a significant influence from the stress concentration of the large pore that is beneath the indentation, which is consistent with the observed effect of a similar sized pore in the experimental data (see Figure 1). The continuum FE layer does not capture this behaviour.

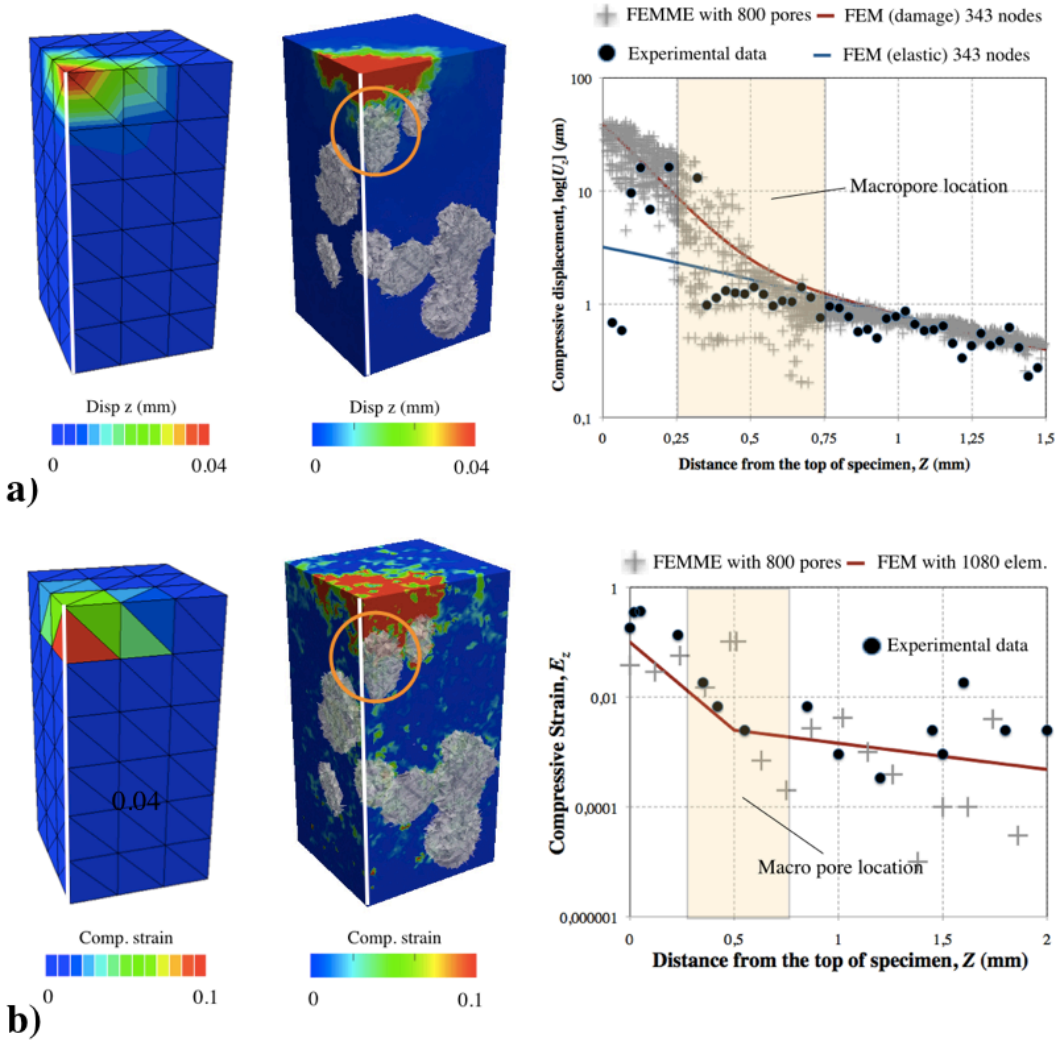

Figure 9: Comparison between the numerical and experimental a) vertical compressive displacement and b) vertical compressive strain; from left to right FEM simulation with damage, FEMME simulation, and comparison of the data.

The global pattern of deformation is therefore similar in the FEMME and FE layer simulations, but the inclusion of microstructure provides a higher fidelity description of the localisation of damage. This is a necessary ingredient of a model that can capture the effects of microstructure in damage propagation and failure of the composite material; such a model could be used to investigate the effects of microstructure on the statistical scatter of strength, for example. For instance, model input data might be obtained from small specimen tests, such as indentation that can be performed at elevated temperatures with irradiated materials, in order to predict the sensitivity to microstructure of damage development in nuclear materials operating in extreme conditions. Parallelisation of the FEMME computations will increase the efficiency compared to FEM simulations of similar fidelity and discretization.

Conclusion

The FEMME methodology can introduce microstructure into a continuum FE model, and successfully reproduces the general features observed in the experimental data of Hertzian indentation in a SiC-SiC_{fibre} composite, observed using high-resolution computed synchrotron X-ray tomography, with the three-dimensional full field displacements measured by digital volume correlation.

Acknowledgements

This work was carried out with the support of the UK EPSRC project "QUBE: Quasi-Brittle fracture: a 3D Experimentally-validated approach" (EP/J019992/1) and also contributes to the Joint Programme on Nuclear Materials (JPNM) of the European Energy Research Alliance (EERA). The authors acknowledge the beam time award at the Joint Engineering, Environmental and Processing (I12) beamline (Experiment EE7730) and the help of Dr H. Çetinel and Mr S. Barhli to conduct the experiment. MM and TJM gratefully acknowledge the support of Oxford Martin School and MM acknowledges the support of Linacre College, Oxford through a Junior Research Fellowship. The Manchester X-Ray Imaging Facility (Dr S.A. McDonald and Professor P.M. Mummery) are thanked for the loan of the loading rig.

References

[1] S.J. Zinkle, G.S. Was (2013), "Materials challenges in nuclear energy", *Acta Materialia*, 61, 735–758

[2] W. E. Lee, M. Gilbert, S. T. Murphy, R. W. Grimes, (2013), "Opportunities for Advanced Ceramics and Composites in the Nuclear Sector". *Journal of the American Ceramic Society*, 96: 2005–2030. doi: 10.1111/jace.12406

[3] J. D. Stempien, D. M. Carpenter, G. Kohse, M. S. Kazimi (2013), "Characteristics of composite Silicon Carbide fuel Cladding After Irradiation under simulated PWR conditions", *Nuclear technology*, 183, pp. 13-29

[4] L Giancarli, J.P Bonal, A Caso, G Le Marois, N.B Morley, J.F Salavy (1998), "Design requirements for SiC/SiC composites structural material in fusion power reactor blankets", *Fusion Engineering and Design*, 41, pp. 165-171.

[5] M. Desaeger, I. Verpoest, (1993), "On the use of the micro-indentation test technique to measure the interfacial shear strength of fibre-reinforced polymer composites.", *Compos Sci Technol.,* 48, pp. 215-226.

[6] D.B. Marshall, W.C. Oliver, (1987), "Measurement of interfacial mechanical properties in fiber-reinforced ceramic composites.", *J. Am. Ceram. Soc*., 70 [8], pp. 542-548.

[7] Bay BK, Smith TS, Fyhire DP, Saad M. Digital volume correlation: three-dimensional strain mapping using X-ray tomography. Exp Mech. 1999;39:217-26

[8] Mostafavi M, Baimpas N, Tarleton E, Atwood RC, McDonald SA, Korsunsky AM, et al. Thre-dimensional crack observation, quantification and simulation in a quasi-brittle material. Acta Mater. 2013;61:6276-89.

[9] Mostafavi M, McDonald SA, Çetinel H, Mummery PM, Marrow TJ. Flexural strength and defect behaviour of polygranular graphite under different states of stress. Carbon. 2013;59:325-36.

[10] Mostafavi M, McDonald SA, Mummery PM, Marrow TJ. Observation and quantification of three-dimensional crack propagation in poly-granular graphite. Eng Fract Mech. 2013;110:410-20.

[11] Roux S, Hild F, Viot P, Bernard D. Three-dimensional image correlation from X-ray computed tomography of solid foam. Compos Pt A-Appl Sci Manuf. 2008;39:1253-65.

[12] Réthoré J, Limodin N, Buffière JY, Hild F, Ludwig W, Roux S. Digital volume correlation analyses of synchrotron tomographic images. J Strain Anal Eng Des. 2011;46:683-95

[13] Vertyagina Y, Mostafavi M, Reinhard C, Atwood RC, Marrow TJ. In situ quantitative three-dimensional characterisation of sub-indentation cracking in polycrystalline alumina. JOURNAL OF THE EUROPEAN CERAMIC SOCIETY. 2014; Volume 33, Issues 15 – 16, December 2013, Pages 3085 – 3093

[14] Mostafavi M, McDonald SA, Mummery PM, Marrow TJ. Observation and quantification of three-dimensional crack propagation in poly-granular graphite. Eng Fract Mech. 2013;110:410-20.

[15] M. Mostafavi, D.M. Collins, B. Cai, R. Bradley, R.C. Atwood, C. Reinhard, P.D. Lee and T.J. Marrow .Yield behaviour beneath hardness indentations in ductile metals, measured by three-dimensional computed X-ray tomography and digital volume correlation. Accepted for publishing in acta materilia.

[16] A.E. Giannakopoulos, S. Suresh, (1997), "Indentation of solids with gradients in elastic properties: part I. Point force", *Int. J Solids Structures*, 34 [19], pp. 2357-2392

[17] M. Zidi, L. Carpentier, A. Chateauminois, F. Sidoroff, (2000), "Quantitative analysis of the micro-indentation behaviour of fibre-reinforced composites: development and validation of an analytical model", *Compos Sci Technol*, 60, pp. 429-437.

[18] G. Aiello, H. Golfier, J.F. Maire, Y. Poitevin, J.F. Salavy, (2000), "Modelling of SiCf/SiC composite structures for nuclear components", *Fusion Eng Des*, 51-52, pp. 73-79

[19] H. Ismar, F. Schroter, F. Streicher, (2000), "Modeling and numerical simulation of the mechanical behavior of woven SiC/SiC regarding a three-dimensional unit cell", *Comp Mater Sci*, 19, pp. 320-328

[20] V. Kouznetsova, M.G.D. Geers, W.A.M. Brekelmans, (2002), "Multi-scale modelling of heterogeneous materials with a gradient-enhanced computational homogenization scheme", *Int J Numer Meth Engng*, 54, pp. 1235-1260.

[21] A. Shterenlikht, I.C. Howards, (2006). "The CAFE model of fracture: application to a TMCR steel." *Fatigue Fract Eng M,* 29, pp. 770-787.

[22] L. Saucedo-Mora, T. J. Marrow, (2015) "FEMME : a multi-scale Finite Element Microstructure MEshfree fracture model for quasi-brittle materials with complex microstructures", *Eng. Fract. Mech.,* In Press, doi:10.1016/j.engfracmech.2015.05.059

[23] S. Zhao, X. Zhou, J. Yu, P. Mummery, (2013), "Effect of heat treatment on microstructure and mechanical properties of PIP-SiC/SiC composites.", *J. Material Sci. and Eng.*, 559, pp. 808-811.

[24] B. Münch, P. Trtik, F. Marone, M. Stampanoni, (2009), "Stripe and ring artifact removal with combined wavelet-Fourier filtering", *Optics Expr.*, 17, pp. 8567-8591.

[25] DaVis. User's manual, (2012), Gottingen: LaVision GmbH

[26] M. A. Sutton, W. J. Wolters, W. H. Peters, W. F. Ranson and S. R. McNeill, (1983), "Determination of displacements using improved digital correlation method" *Image Vis. Comput.* 1, pp. 133–139

[27] C.G. Sammis, M.F. Ashby, (1986). "The failure of brittle porous solids under compressive stress states", Acta metall. 34 [3], pp.

[28] N.A. Fleck, (1997), "Compressive failure of fiber composites.", *Advances in applied mechanics, Academic press*, vol 33

[29] M. Dahan, J. Zarka, (1977), "Elastic contact between a sphere and a semi infinite transversely isotropic body", *Int J solids Structures*, 13, pp. 229-238

[30] M.J. Matthewson, (1981), "Axi-symmetric contact on thin compliant coatings", *J Mech Phys Solids*, 29 [2], pp. 89-113

[31] L.S. Brezeanu, (2014), "Contact stresses: analysis by finite element method (FEM)", *Procedia Technology*, 12, pp. 401-410

[32] S. Suresh, A.E. Giannakopoulos, J. Alcalá, (1997), "Spherical indentation of compositionally graded materials: theory and experiments", *Acta Metall*, 45 [4], pp. 1307-1321

[33] A. Negrea, N.V. Predoi, (2012), "The elastic contact of a sphere with an elastic half-space, a comparison between analytical and finite elements solutions", U.P.B. Sci Bull, Series A, 4 [74], pp.69-78

[34] D.A.W. Kaute, M.F. Ashby, (1994), "Compressive failure of ceramic matrix composites", *Univ. of Cambridge, Dep Engineering*

[35] L. Saucedo-Mora, T.J. Marrow (2015), "Method for the explicit insertion of microstructure in Cellular Automata Finite Element (CAFE) models based on an irregular tetrahedral Finite Element mesh: Application in a multi-scale Finite Element Microstructure MEshfree framework (FEMME)", Finite Elements in Analysis and Design, 105, pp. 56-62

[36] L. Saucedo-Mora, K. Slámečka, U. Thandavamoorthy, T.J. Marrow (2015), "Multi-scale modeling of damage development in a thermal barrier coating", Surface & Coatings Technology, 276, pp. 399-407